MARTIN MARIETTA ENERGY SYSTEMS LIBRARIES

3 4456 0064792 2

ORNL/TM-9992

ornl

OAK RIDGE NATIONAL LABORATORY

MARTIN MARIETTA

Helium Mass Flow Measurement in the International Fusion Superconducting Magnet Test Facility

L. R. Baylor

OAK RIDGE NATIONAL LABORATORY
CENTRAL RESEARCH LIBRARY
CIRCULATION SECTION
4500N ROOM 175
LIBRARY LOAN COPY
DO NOT TRANSFER TO ANOTHER PERSON
If you wish someone else to see this report, send in name with report and the library will arrange a loan.

OPERATED BY
MARTIN MARIETTA ENERGY SYSTEMS, INC.
FOR THE UNITED STATES
DEPARTMENT OF ENERGY

Printed in the United States of America. Available from
National Technical Information Service
U.S. Department of Commerce
5285 Port Royal Road, Springfield, Virginia 22161
NTIS price codes—Printed Copy: A03; Microfiche A01

This report was prepared as an account of work sponsored by an agency of the United States Government. Neither the United States Government nor any agency thereof, nor any of their employees, makes any warranty, express or implied, or assumes any legal liability or responsibility for the accuracy, completeness, or usefulness of any information, apparatus, product, or process disclosed, or represents that its use would not infringe privately owned rights. Reference herein to any specific commercial product, process, or service by trade name, trademark, manufacturer, or otherwise, does not necessarily constitute or imply its endorsement, recommendation, or favoring by the United States Government or any agency thereof. The views and opinions of authors expressed herein do not necessarily state or reflect those of the United States Government or any agency thereof.

ORNL/TM-9992
Dist. Category UC-20

Fusion Energy Division

HELIUM MASS FLOW MEASUREMENT IN THE INTERNATIONAL FUSION SUPERCONDUCTING MAGNET TEST FACILITY

L. R. Baylor

Date Published - August 1986

Prepared by the
OAK RIDGE NATIONAL LABORATORY
Oak Ridge, Tennessee 37831
operated by
MARTIN MARIETTA ENERGY SYSTEMS, INC.
for the
U.S. DEPARTMENT OF ENERGY
under Contract No. DE-AC05-84OR21400

MARTIN MARIETTA ENERGY SYSTEMS LIBRARIES
3 4456 0064792 2

CONTENTS

ACKNOWLEDGMENTS v
ABSTRACT vii
1. INTRODUCTION 1
2. PRINCIPLES OF FLUID FLOW MEASUREMENT 1
   2.1 THEORETICAL DERIVATION 1
   2.2 CORRECTIONS TO THE THEORETICAL EQUATIONS 3
      2.2.1 Discharge Coefficient 3
      2.2.2 Thermal Expansion 4
3. HELIUM FLOWMETERS FOR IFSMTF 4
   3.1 VENTURI TUBE 5
   3.2 ORIFICE PLATE 5
   3.3 INSTALLATION 7
      3.3.1 Cavitation 7
      3.3.2 Length of Straight Pipe 7
4. HELIUM FLOW DATA COLLECTION AND ANALYSIS 7
   4.1 LCPDAS 8
   4.2 HEAT FLOW 8
5. ACCURACY AND EXAMPLES OF IFSMTF MASS FLOW DATA 10
   5.1 ACCURACY 10
   5.2 EXPERIMENTAL DATA 11
6. CONCLUSIONS 11
REFERENCES 13
APPENDIXES
A. EXPANSION FACTOR COMPARISON 15
   A.1 INTEGRAL CALCULATION 15
   A.2 COMPARISON 16
B. LCPDAS HELIUM MASS FLOW CALCULATION ROUTINES 19

ACKNOWLEDGMENTS

The author wishes to thank L. Dresner for many useful discussions on the thermodynamics of helium and for reviewing this manuscript. P. L. Walstrom is acknowledged for his specification and calibration of the flowmeters used.

ABSTRACT

The measurement of helium mass flow in the International Fusion Superconducting Magnet Test Facility (IFSMTF) is an important aspect in the operation of the facility's cryogenic system. Data interpretation methods that lead to inaccurate results can cause severe difficulty in controlling the experimental superconducting coils being tested in the facility. This technical memorandum documents the methods of helium mass flow measurement used in the IFSMTF for all participants of the Large Coil Program and for other cryogenic experimentalists needing information on mass flow measurements. Examples of experimental data taken and calculations made are included to illustrate the applicability of the methods used.

1. INTRODUCTION

The International Fusion Superconducting Magnet Test Facility (IFSMTF) has been designed and built at the Oak Ridge National Laboratory (ORNL) for the purpose of testing prototype superconducting toroidal field coils that are approximately half-scale for a tokamak fusion reactor.[1] The test coils have been provided through international collaboration by the United States, EURATOM, Japan, and Switzerland and are being tested in a six-coil compact torus. The test coils have bore dimensions of 2.5 × 3.5 m and a weight of 40–45 tonnes. Each coil is designed to produce a peak field of 8.0 T.

The test facility consists of an 11-m-diam vacuum tank and is cooled with a liquid nitrogen (LN) system and a helium refrigeration system. The helium system is designed to provide a cooldown flow of 300 g/s of helium gas with a temperature between 300 and 80 K. During operation, liquid helium at 4.2 K is provided to the bath-cooled coils and test stand; at the same time, 300 g/s of 3.8 K helium at supercritical pressures up to 1.5 MPa (15 atm) is provided to the forced-flow coils. Operation of the helium system is carefully integrated with coil testing in order to minimize thermal stresses during cooldown and to provide adequate liquid and cooling to keep the coils in their superconducting state. Accurate measurements of helium flows and heat loads are required over a wide range of operating parameters to ensure cryostable and efficient operation.

The measurement of fluid flow in closed conduits is widely practiced in process industries and is generally well understood. The unique feature of helium mass flow measurement in IFSMTF is the wide range of thermodynamic conditions under which the flow must be measured. This feature necessitates the calculation of thermodynamic properties of helium from the measured helium temperature and pressure in order to get accurate mass flow results over the entire range of conditions.

2. PRINCIPLES OF FLUID FLOW MEASUREMENT

2.1 THEORETICAL DERIVATION

When viscous stresses and heat transfer are suppressed, the quantity $(h + u^2/2)$ is a constant along a streamline in a tube of steady flow with no elevation difference, where h is the specific enthalpy (enthalpy per unit mass) and u is the fluid velocity.[2] For the case shown in Fig. 1, the idealized isentropic flow is given by Bernoulli's equation:

$$u_1^2/2 - u_2^2/2 + h_1 - h_2 = 0 \ . \tag{1}$$

The conservation of mass is given by

$$\dot{m} = \rho_1 A_1 u_1 = \rho_2 A_2 u_2 \ , \tag{2}$$

where ρ is the density of the fluid and A is the cross-sectional area. By solving Eq. (2) for u_1 and u_2 and inserting into Eq. (1), one gets

ORNL-DWG 86-2108 FED

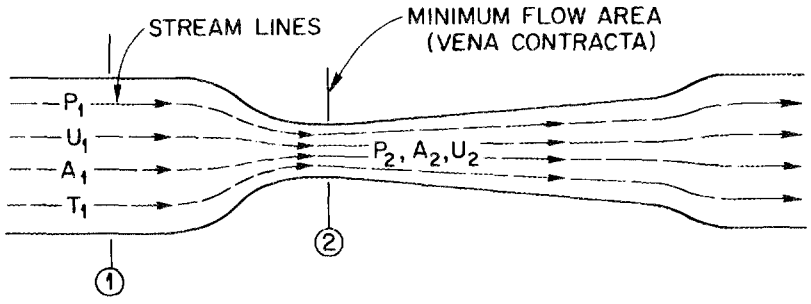

Fig. 1. Idealized flow through a restriction.

$$\dot{m} = A_2\rho_2\left\{2(h_1 - h_2)/[1 - (A_2\rho_2/A_1\rho_1)^2]\right\}^{1/2} \tag{3}$$

for the mass flow. Equation (3) may be written in terms of pressure drop by noting that for isentropic processes[3]

$$dh = \frac{1}{\rho}dP \ , \tag{4}$$

where P is the pressure. Thus,

$$\dot{m} = A_2\rho_2\left\{2\int_{P_2}^{P_1}\frac{1}{\rho}dP/[1 - (A_2\rho_2/A_1\rho_1)^2]\right\}^{1/2} \ , \tag{5}$$

where the integral is evaluated along a line of constant entropy, since Eq. (4) applies to an isentropic process.

The pressure and volume of an ideal gas (e.g., helium above 20 K at 1 MPa) are related at constant entropy by the equation

$$Pv^{\gamma} = P\left(\frac{1}{\rho}\right)^{\gamma} = \text{constant} \ , \tag{6}$$

where v is the specific volume and γ, the isentropic exponent, is the ratio of specific heat at constant pressure to specific heat at constant volume (C_P/C_v). By using Eq. (6) to evaluate the integral in Eq. (5) one gets the expression[4]

$$\dot{m}^2 = 2A_2^2\tau^{2/\gamma}\rho_1 P_1\left(\frac{\gamma}{\gamma-1}\right)\left[1-\tau^{(\gamma-1)/\gamma}\right]\Big/\left[1-(A_2/A_1)^2\tau^{2/\gamma}\right] , \tag{7}$$

which is known as the theoretical adiabatic mass flow equation, where τ is the pressure ratio P_2/P_1. For incompressible flow (e.g.. ρ is constant), Eq. (5) yields the expression

$$\dot{m}^2 = 2A_2^2(P_1 - P_2)\rho_1\Big/[1-(A_2/A_1)^2] = \frac{2A_2^2\Delta P\rho_1}{1-(A_2/A_1)^2} . \tag{8}$$

It is common to write Eq. (7) in the form

$$\dot{m}^2 = \epsilon^2 2A_2^2(P_1 - P_2)\rho_1\Big/\left[1-(A_2/A_1)^2\right] , \tag{9}$$

where ϵ, called the expansion factor, is less than unity and is equal to the ratio of the square roots of the right-hand sides of Eqs. (7) and (8). With some simplification, the expression for the expansion factor can be written as:

$$\epsilon = \left\{\left(\frac{\gamma}{\gamma-1}\tau^{2/\gamma}\right)\left[\frac{1-A_2^2/A_1^2}{1-\tau^{2/\gamma}(A_2/A_1)^2}\right]\left[\frac{1-\tau^{(\gamma-1)/\gamma}}{1-\tau}\right]\right\}^{1/2} . \tag{10}$$

By defining β, the diameter ratio, as $d/D = (A_2/A_1)^{1/2}$, Eq. (10) can be rewritten as:

$$\epsilon = \left\{\left(\frac{\gamma}{\gamma-1}\tau^{2/\gamma}\right)\left[\frac{1-\beta^4}{1-\tau^{2/\gamma}\beta^4}\right]\left[\frac{1-\tau^{(\gamma-1)/\gamma}}{1-\tau}\right]\right\}^{1/2} . \tag{11}$$

2.2 CORRECTIONS TO THE THEORETICAL EQUATIONS

In addition to the expansion factor derived in Sect. 2.1, the viscous stresses, heat transfer effects, and pressure tap locations must also be taken into account for accurate mass flow measurement.[4]

2.2.1 *Discharge Coefficient*

A factor known as the discharge coefficient, a measure of the flow's departure from the theoretical flow rate, is included in the expression for mass flow. The expression can be written as:

$$\dot{m} = \epsilon CE \frac{\pi}{4} d^2 (2\Delta P \rho)^{1/2} \ , \tag{12}$$

where E is the velocity of approach factor $1/(1 - \beta^4)^{1/2}$ and C is the discharge coefficient. Note also that A_2 has been rewritten as $(\pi/4)d^2$. In general, C cannot be calculated and must be determined by experiment. In some flow equations the discharge coefficient is combined with the velocity of approach factor and redefined as the flow coefficient. The flow coefficient is then defined as

$$\alpha_{Fc} = \frac{C}{\sqrt{1 - \beta^4}} = EC \ . \tag{13}$$

2.2.2 *Thermal Expansion*

Another correction factor which must be applied is the thermal expansion factor. The material of the pipe and the flow element expand or contract with temperature, which affects the pipe and orifice diameters. The thermal expansion factor F_α is used to correct for these effects. When the thermal expansion coefficients α_{TE} of the flow element and pipe are approximately the same, the thermal expansion correction factor is given by[4]

$$F_\alpha = 1 + 2\alpha_{TE}(T_K - 293.15) \ . \tag{14}$$

As an example, a 300-series stainless steel element that has a thermal expansion coefficient of 0.0133 μm/mm·K would have a thermal expansion factor F_α of 0.9923 at 4 K.

The complete expression for mass flow rate, including the discharge coefficient and the thermal expansion factor, then becomes:

$$\dot{m} = \epsilon F_\alpha CE \frac{\pi}{4} d^2 (2\Delta P \rho)^{1/2} \ . \tag{15}$$

3. HELIUM FLOWMETERS FOR IFSMTF

The orifice plate and venturi tube are the two primary types of flowmeters used to measure helium flow in the cryogenic system of the IFSMTF. The venturi flowmeters are used in the forced-flow coil and helium purifier circuits because of their inherently low unrecoverable pressure drop. The flow rates in the pool boiling and cooldown circuits are measured with orifice plates because of their simplicity of manufacture and installation. The unrecoverable pressure drop is significantly higher in the orifice plate than in the venturi meter because of the different discharge coefficients of the two types of flowmeters.

3.1 VENTURI TUBE

The venturi flowmeters used in the IFSMTF helium system are classical venturi tubes with machined convergent entrance and exit cones.[5] A diagram of the geometric profile of the venturi meters is shown in Fig. 2. The venturi meters are manufactured from 304L austenitic stainless steel and have an internally smooth finish. The pressure taps are located at the vena contracta or throat and at the entrance.

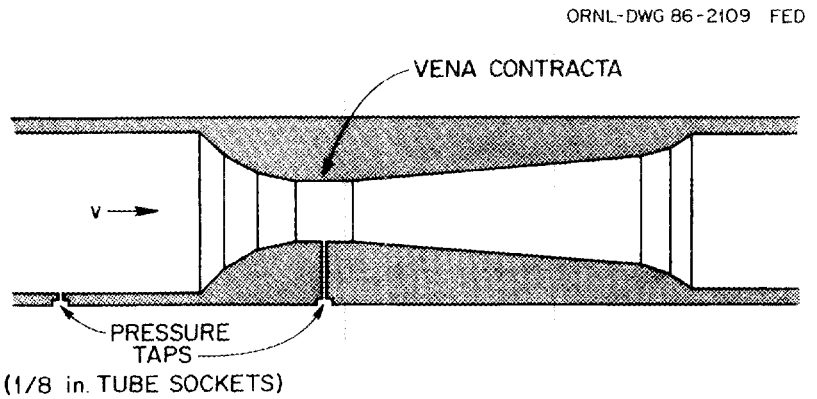

Fig. 2. Venturi tube profile.

The discharge coefficient for the classical venturi tube with a machined convergent entrance varies from 0.996 at a Reynolds number greater than 5.0×10^5 (low-temperature conditions) to 0.96 at Reynolds numbers below 1.0×10^5 (room temperature). Since the highest accuracy is desired at low-temperature conditions in IFSMTF, the discharge coefficient is assumed to be a constant 0.995.

For venturis, the gas expansion is assumed to be purely axial. For these devices there is excellent experimental agreement with the adiabatic gas expansion factor. At low temperature and high pressure, supercritical helium is not an ideal gas; therefore the expansion integral in Eq. (5) has been calculated explicitly and compared to the ideal adiabatic gas expansion factor [Eq. (10)]. The difference between using the integral and using the expansion factor in the mass flow equation is shown in Appendix A to be very small over the range of temperature and pressure used in the IFSMTF; therefore, the adiabatic gas expansion factor is used in calculating venturi mass flow rates for all helium conditions.

3.2 ORIFICE PLATE

The orifice plates used in the IFSMTF helium system are circular and concentric with the pipe centerline and have flat and parallel faces. A diagram of an orifice plate is shown in Fig. 3. The orifice plates, manufactured from 304L austenitic stainless steel, are welded into the pipe. The pressure taps are corner taps that break through the wall flush with the faces of the plate. The discharge coefficient for the corner-tap orifice plate has been empirically determined to be given by the Stolz equation:[6]

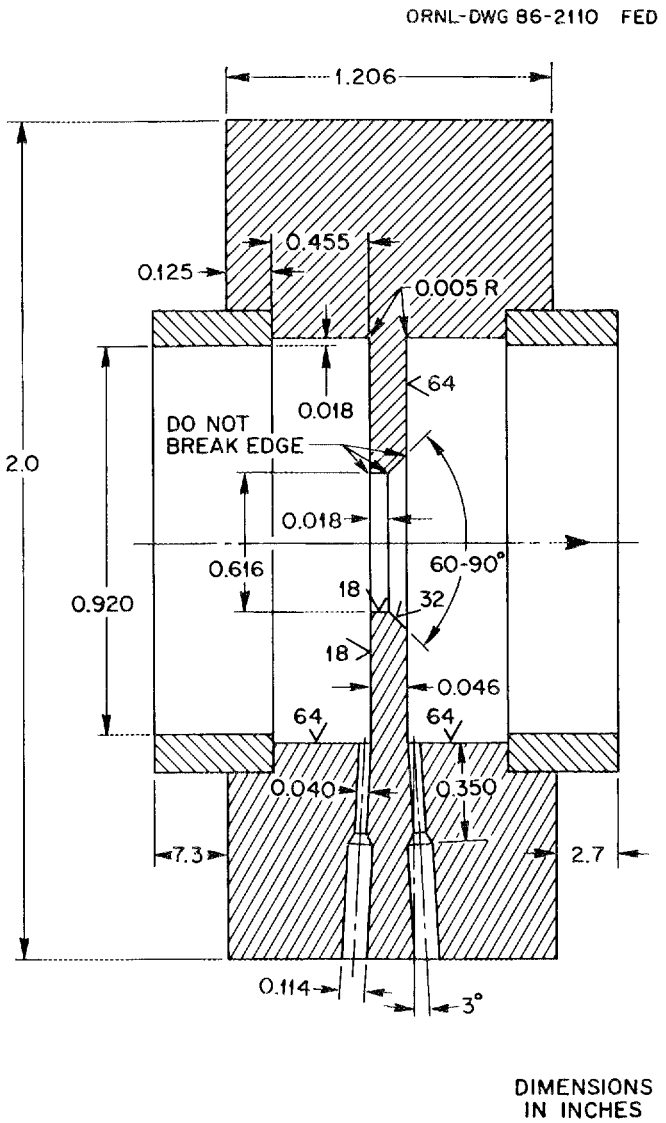

Fig. 3. Orifice plate design used in IFSMTF.

$$C = 0.5959 + 0.312\beta^{2.1} - 0.1840\beta^{8} + 0.0029\beta^{2.5}\left(\frac{10^6}{\mathrm{Re}_D}\right)^{0.75} . \tag{16}$$

For a square-edged orifice, such as those used in the IFSMTF, gas expansion is both radial and axial, and an empirically determined expansion factor is used instead of the adiabatic gas expansion factor. The orifice expansion factor derived by Buckingham[4] is

$$\epsilon = 1 - (0.41 + 0.35\beta^4)\frac{\Delta P}{\gamma P} \tag{17}$$

and is applicable in the range of use for helium in the IFSMTF.

3.3 INSTALLATION

Both types of flowmeters are installed in the system by welding the units into the process piping. Since the system is cryogenic, the piping, including the flowmeters, is insulated from radiative heat with superinsulation. Small-diameter, thin-wall stainless steel tubing is welded into the pressure tap sockets of the flowmeters and is wrapped around the process piping several turns for improved heat sinking. The tubing is routed at a slight incline to a vacuum flange, where the connections are made to the differential pressure and pressure instrumentation. The tubing must be insulated from radiative heat and must also be routed at an incline to minimize acoustic oscillations.

3.3.1 *Cavitation*

The effects of cavitation (boiling of the process liquid, caused by a decrease in the pressure to the vapor pressure) must be considered in the design of any flow measurement system. The collapse of the vapor cavities formed in the fluid by cavitation can damage piping and flowmeters. In the IFSMTF, the process fluid is helium gas or supercritical helium, and cavitation does not occur from pressure drop in the flowmeters. When liquid helium is introduced into the system, the flow rate is so low that the pressure does not fall below the vapor pressure to cause any appreciable cavitation.

3.3.2 *Length Of Straight Pipe*

In order to ensure that the velocity of the fluid at the flowmeter is primarily axial and swirl free, a long length of straight pipe must be upstream of the flowmeter.[6] In the IFSMTF, the helium piping was designed to accommodate at least 20 pipe diameters of straight length upstream of all flowmeters.

4. HELIUM FLOW DATA COLLECTION AND ANALYSIS

It can be seen from the formula derived for mass flow in Sect. 2 that the differential pressure across the flow element and the density of the helium in the flow element must be known in order to calculate the mass flow rate. The differential pressure is measured directly by a differential pressure transducer that works on a variable capacitance principle. Density cannot be measured directly and must be calculated from the temperature and pressure measurements using the known thermodynamic properties of helium. The pressure is measured directly with a strain gage transducer, and the temperature is measured with a type E thermocouple for temperatures above 77 K and with a carbon glass resistance thermometer for lower temperatures. The analog voltages from these transducers are read by the data acquisition system, and computer programs are used to calculate the mass flow rates. A block diagram of the instrumentation used for mass flow measurement is shown in Fig. 4.

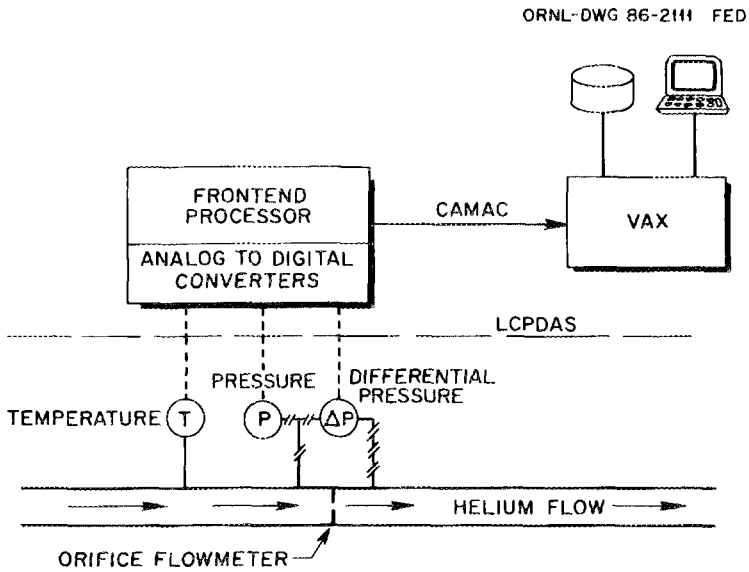

Fig. 4. Block diagram of mass flow measurement instrumentation.

4.1 LCPDAS

The Large Coil Project data acquisition system (LCPDAS) is a VAX 11/780 minicomputer-based system designed for the acquisition, storage, and retrieval of experimental IFSMTF data.[7] The analog signals from instrumentation in the facility are interfaced to four front-end processors that convert the data from analog to digital form, which is acquired by the VAX through a CAMAC serial highway. The VAX archives the data on magnetic disk media and makes the information available for a variety of application programs to display and analyze.

A software mechanism has been implemented in the LCPDAS to enable the retrieval of pseudo-sensors using data from archived data files or real-time data buffers. Pseudo-sensors calculate a user-defined physical parameter using actual measurements from multiple real sensors. The pseudo-sensors are defined in a utility program, and routines for calculating the physical parameter are used in the data retrieval software to retrieve pseudo-sensor data. Helium mass flow is one of the many pseudo-sensor calculations available to users of the LCPDAS. Helium properties such as density, viscosity, and enthalpy are also available as pseudo-sensors.

4.2 HEAT FLOW

One important pseudo-sensor calculation that deserves mention is heat flow through a section of the cryogenic system. In an isobaric process, the heat that is transferred is the change of enthalpy;[3] that is,

$$H_f - H_i = Q \ , \tag{18}$$

where H is the enthalpy and Q is the heat. By calculating the specific enthalpy at two points of approximately the same pressure and calculating the mass flow through the system, it is possible to calculate the heat flow with

$$(h_f - h_i)\dot{m} = \dot{Q} \ . \tag{19}$$

The heat flow calculation routine in the LCPDAS calculates the specific enthalpy at two locations in the cryogenic system and uses one orifice plate mass flow calculation to derive the heat flow.

The calculation routines from the LCPDAS for calculating helium mass flow rates from venturi meters and orifice plates and the routine for calculating heat flow are included in Appendix B. The routines are written in VAX-11 PASCAL and use the HEPROP FORTRAN subroutines from Oxford University[8] to calculate the thermophysical properties of helium. The thermodynamic properties are derived in HEPROP from equations of state developed by McCarty[9] and are valid at temperatures from 2 K to 1700 K and at pressures up to 100 MPa, as shown in Fig. 5.

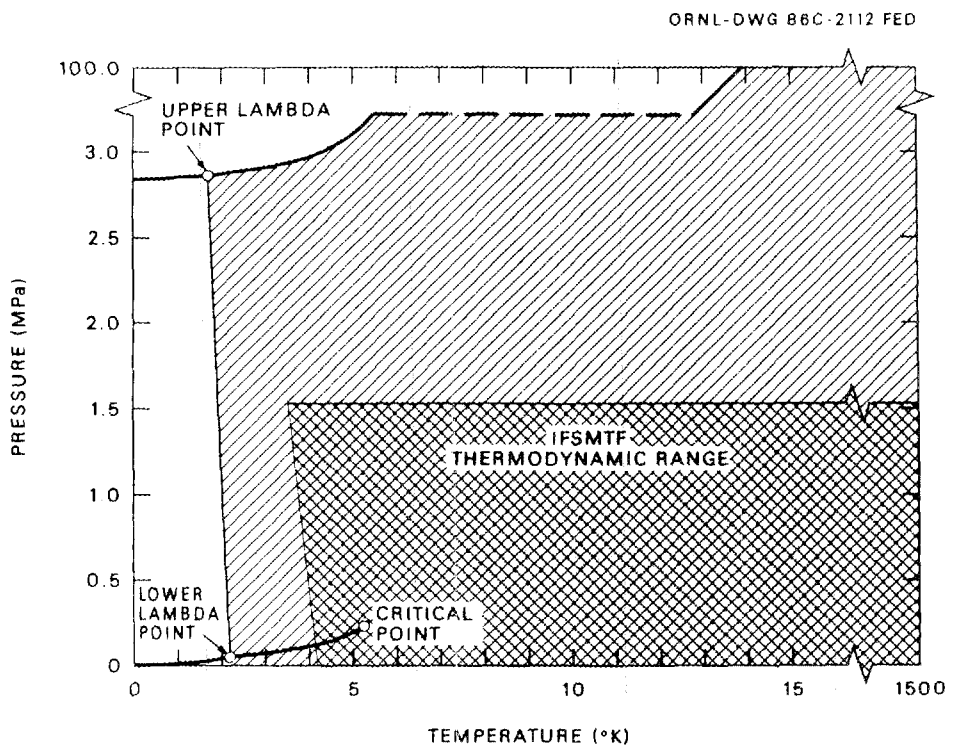

Fig. 5. Range of validity for HEPROP.

5. ACCURACY AND EXAMPLES OF IFSMTF MASS FLOW DATA

Much data has been and will continue to be collected from the Large Coil Program. The mass flow data are used in operating the facility and in analyzing the thermodynamic properties of the superconducting coils.

5.1 ACCURACY

The measurement of mass flow rate has inherent errors, as do all measurements. To determine mass flow rate measurement accuracy, the accuracy of the flowmeter must be combined with the individual accuracies of the instruments used to measure temperature, pressure, and differential pressure and then properly weighed in the mass flow rate calculation. The accuracy of the temperature measurement is affected by the location of the temperature sensor on the outside of the pipe and its thermal conductivity with the helium. The static temperature of the moving helium is assumed to be equal to the indicated temperature. The pressure and differential pressure transducers are calibrated with accurate gages traceable to NBS standards.

A simplified method of estimating the mass flow rate measurement accuracy Acc is the root-sum-square method:[4]

$$\mathrm{Acc} = [(X_T)^2 + (X_P)^2 + (X_{\Delta P})^2 + \cdots]^{1/2} , \tag{20}$$

where the square root of the sum of the squares of individual quantities is taken as the overall accuracy. The quantities that influence the mass flow rate measurement are listed in Table 1 with their estimated accuracies. The overall accuracy of the measurement is then estimated to be the root-sum-square of these accuracies, which is 3.5% and is well within the initial design goal for the IFSMTF of 5%.

Table 1. Mass flow measurement accuracies

Quantity	Estimated accuracy $X(\mathrm{Acc})$ (%)	$[X(\mathrm{Acc})]^2$
Temperature T	2.50	6.2500
Pressure P	1.00	1.0000
Differential pressure ΔP	1.00	1.0000
Density calculation ρ	1.00	1.0000
Discharge coefficient C	1.00	1.0000
Expansion factor ϵ	1.00	1.0000
Thermal expansion factor F_α	0.50	0.2500
Pipe diameter D	0.25	0.0625
Flowmeter diameter d	0.10	0.0100
		11.5725
$\{\Sigma\,[X(\mathrm{Acc})]^2\}^{1/2} = 3.4$		

5.2 EXPERIMENTAL DATA

Examples of the data collected and processed by the mass flow calculation routines are shown in the following plots. In Fig. 6 the temperature, pressure, differential pressure, and calculated helium mass flow rate in grams per second through a venturi flowmeter in the IFSMTF system are shown over a 36-h period. In Fig. 7 the temperature, pressure, differential pressure, and calculated helium mass flow rate through an orifice plate in one of the forced-flow coils are shown over a 16-h period.

As can be seen from the data, the mass flow rate is subject to sudden changes due to the helium refrigerator operating conditions. It is important for the refrigerator operators to monitor the mass flow rate so that the cooldown of the coils and facility may be maintained at a steady rate and not cause any thermal stresses to build up between structural components.

6. CONCLUSIONS

The accurate measurement of helium mass flow in the IFSMTF has been made possible by careful design of the helium and instrumentation systems and by use of known thermophysical properties of helium. The general methods used in the IFSMTF are applicable to other cryogenic systems where there are wide variations in the density of the fluid and where the fluid can be approximately modeled as an ideal gas.

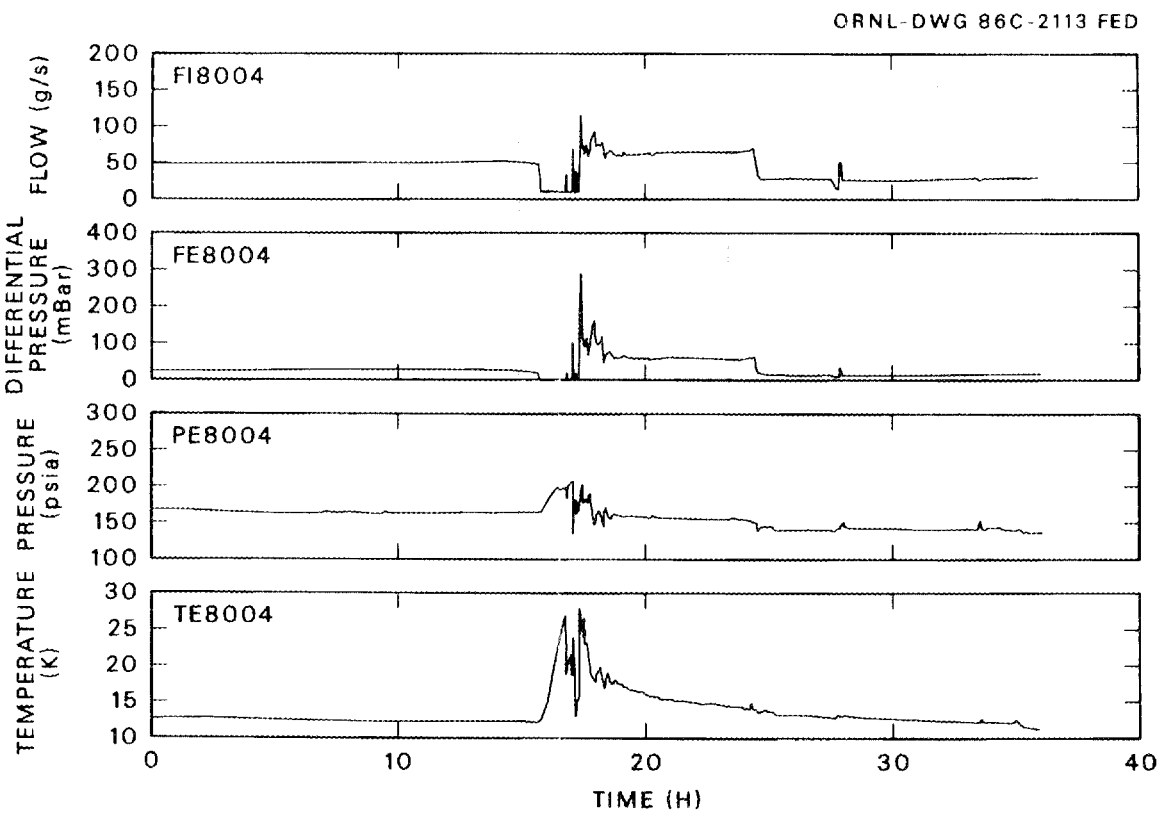

Fig. 6. Mass flow data for venturi flowmeter.

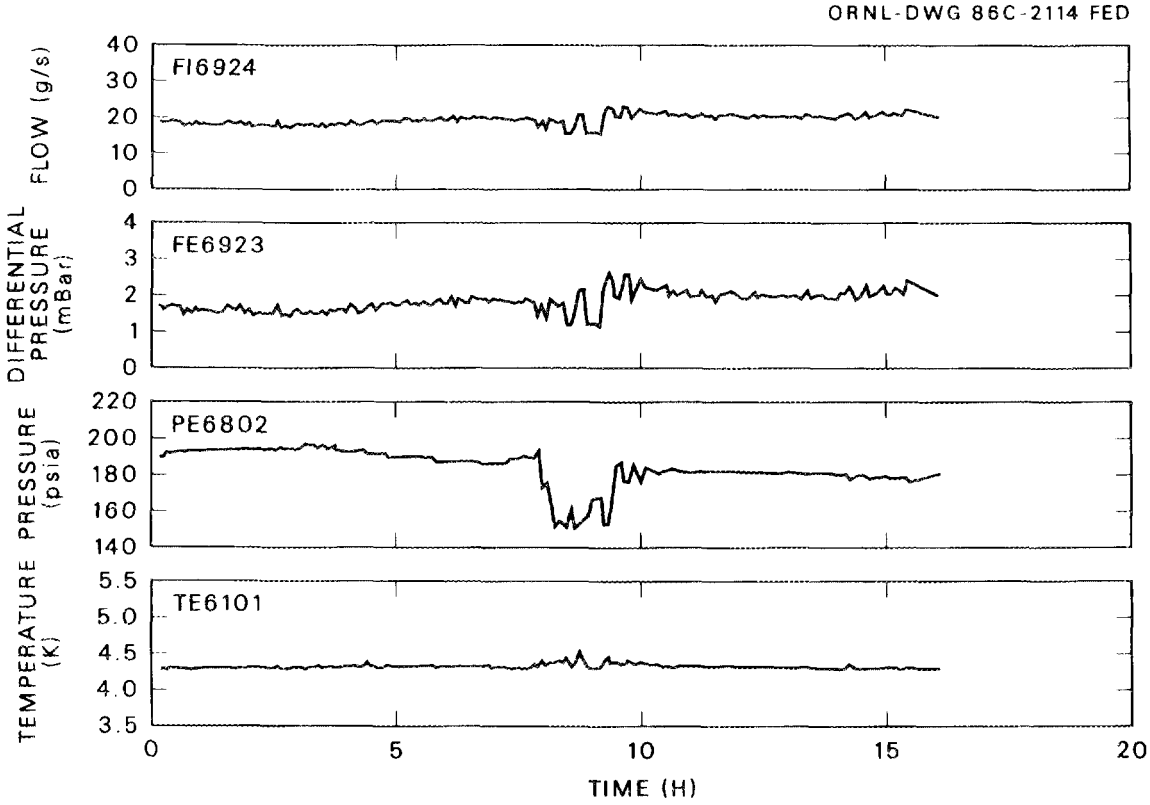

Fig. 7. Mass flow data for orifice flowmeter.

REFERENCES

1. P. N. Haubenreich et al., "Status of the Large Coil Test Facility," pp. 1337–41 in *Proceedings of the 10th Symposium on Fusion Engineering*, IEEE, Piscataway, N.J., 1983.

2. P. A. Thompson, *Compressible-Fluid Dynamics*, McGraw-Hill, New York, 1972, p. 64.

3. M. W. Zemansky and R. H. Dittman, *Heat and Thermodynamics*, McGraw-Hill, New York, 1981, p. 213.

4. R. W. Miller, *Flow Measurement Engineering Handbook*, McGraw-Hill, New York, 1983, Chap. 9.

5. P. L. Walstrom, "Calibration of Venturi Flowmeters for LCTF," unpublished, April 10, 1984.

6. International Standard ISO/5167-1980, International Organization for Standardization, Geneva, 1980.

7. E. T. Blair and L. R. Baylor, "User's Manual for the Large Coil Project Data Acquisition System," unpublished.

8. B. A. Hands, HEPROP, University of Oxford Department of Engineering Science Report 1289/79, April 1979.

9. R. D. McCarty, NBS Technical Note 631, U.S. Department of Commerce, 1972.

Appendix A

EXPANSION FACTOR COMPARISON

In Sect. 2 it was shown that for an ideal gas, the mass flow equation [Eq. (5)] could be rewritten in the form of a theoretical adiabatic mass flow equation [Eq. (8)]. For a non-ideal gas, in particular supercritical helium, it is necessary to use Eq. (5) and solve the expansion integral to get accurate mass flow calculations. This integral was solved using the following method, and the resulting mass flow calculation was compared with the theoretical adiabatic mass flow equation.

A.1 INTEGRAL CALCULATION

The expansion integral is given from Eq. (5) as

$$F = \int_{P_2}^{P_1} \frac{1}{\rho}\, dP \tag{A1}$$

and is evaluated along a line of constant entropy since it applies to an isentropic process. To solve this integral it is necessary to calculate the density from P_1 to P_2, which requires the temperature from P_1 to P_2. The temperature can be calculated by use of the adiabatic condition:

$$dS = 0 = \left(\frac{\partial S}{\partial P}\right)_T dP + \left(\frac{\partial S}{\partial T}\right)_P dT \ . \tag{A2}$$

The first term in Eq. (A2) may be written as

$$\left(\frac{\partial S}{\partial P}\right)_T = -\left(\frac{\partial V}{\partial T}\right)_P = -V\left[\frac{1}{V}\left(\frac{\partial V}{\partial T}\right)_P\right] = -V\beta \ . \tag{A3}$$

The second term in Eq. (A2) may be written as

$$\left(\frac{\partial S}{\partial T}\right)_P = \frac{(dQ/dT)_P}{T} = C_P/T \ . \tag{A4}$$

Thus, Eq. (A2) can be solved for dT, yielding

$$dT = (\beta T/\rho C_P)\, dP \ . \tag{A5}$$

The parameter beta may be calculated in the following way:

$$\beta = \frac{1}{V}\left(\frac{\partial V}{\partial T}\right)_P = -\frac{1}{\rho}\left(\frac{\partial \rho}{\partial T}\right)_P \quad . \tag{A6}$$

From the minus-one chain rule, the parameter beta may be rewritten as

$$\beta = -\frac{1}{\rho}\left[\frac{-1}{(\partial T/\partial P)_\rho\,(\partial P/\partial \rho)_T}\right] = \frac{1}{\rho}\,\frac{(\partial P/\partial T)_\rho}{(\partial P/\partial \rho)_T} \quad , \tag{A7}$$

which can be calculated numerically by HEPROP[1] using DPDT/(DPDD * ρ). The following iteration scheme can then be used to numerically integrate the expansion integral:

$$\Delta P = (P_1 - P_2)/N \quad , \tag{A8}$$

$$P_{n+1} = P_n - \Delta P \quad , \tag{A9}$$

$$T_{n+1} = T_n - \frac{\beta_n\, T_n\, \Delta P}{\rho_n\, C_{P_n}} \quad , \tag{A10}$$

$$F_{n+1} = F_n + \frac{\Delta P}{\rho_n} \quad . \tag{A11}$$

The initial pressure is taken as P_1 and the initial temperature is taken as T_1.

A.2 COMPARISON

The mass flow rate of helium was calculated for a given venturi by using both the theoretical adiabatic mass flow equation and the equation with the expansion integral. In solving the expansion integral, it was verified that the integral was evaluated along a line of constant entropy. The results of both calculations were compared over a range of temperature and pressure expected to be seen in the cryogenic system of the IFMSTF and were plotted in Fig. A.1. The maximum difference between the two calculations is on the order of 1%. It was therefore decided to use the adiabatic mass flow equation for all helium venturi calculations because the solution of the integral uses significantly more computer processing time.

ORNL-DWG 86-2115 FED

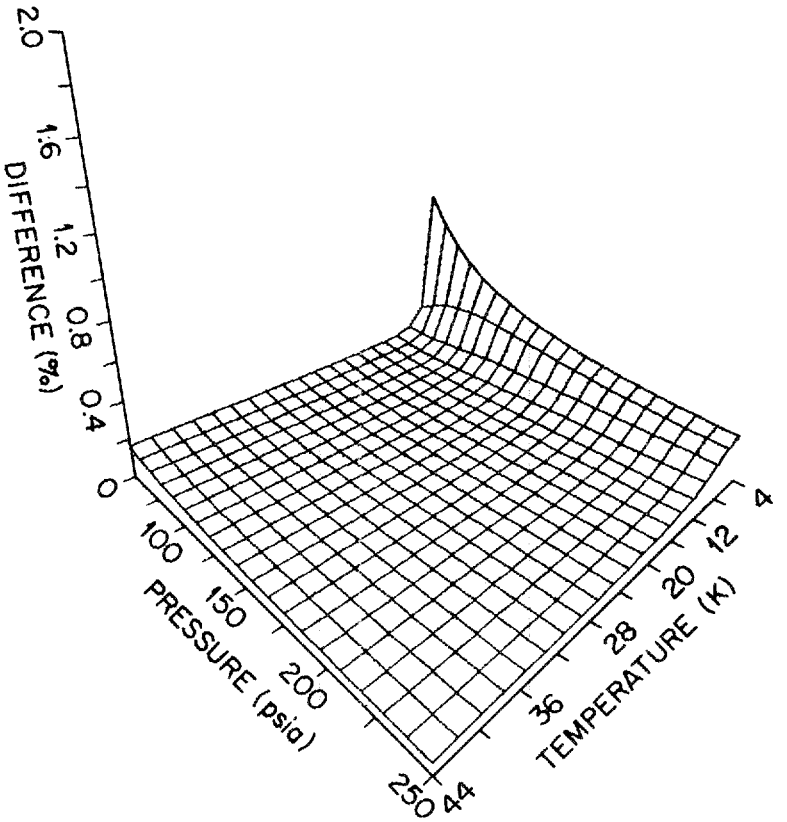

Fig. A.1. Difference in mass flow calculation.

REFERENCE

1. B. A. Hands, HEPROP, University of Oxford Department of Engineering Science Report 1289/79, April 1979.

Appendix B

LCPDAS HELIUM MASS FLOW CALCULATION ROUTINES

```
{**********}
{*
{*   Function heflow_orif: real;
{*
{*   Functional Description:
{*           Function to calculate helium mass flow from
{*           temperature, pressure, and differential pressure in
{*           an orifice plate conforming to ISO 5167-1980.
{*           The massflow is returned in g/s as the function value.
{*           This routine is called as a calculation channel routine.
{*
{*   Formal Parameters:
{*           Sensor_count - integer number of sensor values used. (4)
{*           Sensor_values(1) - temperature value in K (low temp).
{*           Sensor_values(2) - temperature value in K (high temp).
{*           Sensor_values(3) - pressure value in PSIA.
{*           Sensor_values(4) - differential pressure value in mBar.
{*           Sensor_coeffs(1) - inner diameter of pipe in mm.
{*           Sensor_coeffs(2) - inner diameter of orifice throat in mm.
{*           Sensor_coeffs(3) - temperature breakpoint in K.
{*
{*   Implicit Inputs:
{*           convfact1 - conversion factor for PSIA to PASCAL.
{*           convfact2 - conversion factor for mBar to PASCAL.
{*           alpha_ss - thermal expansion coefficient stainless steel.
{*
{*   Implicit Outputs:
{*
{*   Routine Status/Completion Codes:
{*
{*   Side Effects:
{*
{*   Notes:
{*           Reynold's number assumed to be initially 1.0E5.
{*           The massflow calculation is iterated until the
{*           reynold's number converges to within 10%.
{*
{**********}
function heflow_orif
             (var sensor_count: [readonly]integer;
              var sensor_values: [readonly]packed array
                            [$11..$u1: integer] of real;
              var sensor_coeffs: [readonly]packed array
                            [$12..$u2: integer] of real):
             real;

     label
             1111, 9999;                        { Error exit }
     var
             temp_low,temp_high: real;          { sensor values }
             temp,press,deltap: real;           { sensor values }
             temp_bkpt: real;                   { temperature breakpoint }
             idpipe, idthroat: real;            { sensor coefficients }
             dens: real;                        { density KG m**-3 }
             mflow: real;                       { mass flow KG/s }
             ReD: real;                         { Reynold's number }
             diffReD: real;                     { (ReD - newReD)/newReD }
             newReD: real;                      { new calculated value of ReD }
             eta: real;                         { Viscosity N s m**-2 }
             C: real;                           { discharge coefficient }
             alpha: real;                       { Flow coefficient }
             expan: real;                       { Expansion factor }
             beta: real;                        { ratio of d to D }
             aread: real;                       { area of throat }
             m: real;                           { beta squared }
```

```
        cp, cv: real;                       { Cp and Cv }
        gamma: real;                        { Isentropic exponent }
        a: real;                            { constant in alpha }
        F: real;                            { Thermal-expansion factor }

begin   {function heflow_orif}

        { Initialize input parameters }

        temp_low := sensor_values[1];
        if temp_low < 2.Ø then
                temp_low := 2.Ø;
        temp_high := sensor_values[2];
        if temp_high < 2.Ø then
                temp_high := 2.Ø;
        press := sensor_values[3];
        if press <= press_min then
                begin
                heflow_orif := Ø.Ø;
                goto 9999;
                end;
        deltaP := sensor_values[4];
        if deltap <= Ø.Ø then
                begin
                heflow_orif := Ø.Ø;
                goto 9999;
                end;

        idpipe := sensor_coeffs[1];
        idthroat := sensor_coeffs[2];
        temp_bkpt := sensor_coeffs[3];

        { Conversions and factors }
        if temp_high <= temp_bkpt then
                temp := temp_low
        else
                temp := temp_high;

        beta := idthroat/idpipe;            { calc ratio of d to D }
        m := beta**2;                       { m = beta squared }
        aread := ((idthroat/1ØØØ.Ø)**2)*pi/4.Ø;
                                            { area of throat m**2 }
        deltap := convfact2*deltap;         { Convert mBar to Pascal }
        press := convfact1*press;           { Convert PSIA to Pascal }
        dens := dfun (press,temp);          { Heprop density KG/M**3 }
        eta := visc (dens,temp);            { Heprop viscosity N s M**-2 }
        cp := csubp (temp,press);           { Calculate Cp }
        cv := csubv (temp,press);           { Calculate Cv }
        gamma := cp/cv;                     { calc isentropic exponent }
        ReD := 1.ØE5;                       { Start ReD = 1ØØØØ }
        F := 1 + 2* alpha_ss*(temp - 293.15);
                                            { Thermal-expansion factor }

        if (dens<Ø.Ø) or (eta<Ø.Ø) or (cp<Ø.Ø)
                or (cv <Ø.Ø) then
                begin
                heflow_orif := -9999.9;
                goto 9999;
                end;

1111:

        { Discharge coefficient for orifice plate ISO 5167-198Ø }
        C := Ø.5959 + Ø.Ø312*beta**2.1 - Ø.184Ø*beta**8.Ø
                + (Ø.ØØ29*beta**2.5)*(1.ØE6/ReD)**Ø.75;

        { Flow coefficient for orifice plate ISO 5167-198Ø }
        alpha := C * (1 - beta**4.Ø)**(-Ø.5);

        { Expansibility (expansion) factor ISO 5167-198Ø }
        expan := 1 - (Ø.41 + Ø.35*beta**4) * deltap/(press * gamma);
```

```
                { Calculation of mass flow (Kg/s) }
                mflow := alpha*F*expan*aread*((2.Ø*dens*deltap)**Ø.5);

                { Calculate new value of Reynold's number }
                newReD := mflow*4/(pi * eta * (idpipe/1ØØØ.Ø));
                diffReD := (ReD-newReD)/newReD;
                ReD := newReD;
                If diffReD > Ø.1 then
                        goto 1111;

                heflow_orif := mflow * 1ØØØ.Ø;  { massflow in g/s }

9999:
     end;       {function heflow_orif}
```

```
{**********}
{*
{*   Function heflow_vent: real;
{*
{*   Functional Description:
{*           Function to calculate helium mass flow from
{*           temperature, pressure, and differential pressure in
{*           a venturi tube conforming to ISO 5167-1980.
{*           The massflow is returned in g/s as the function value.
{*           This routine is called as a calculation channel routine.
{*
{*   Formal Parameters:
{*           Sensor_count - integer number of sensor values used. (4)
{*           Sensor_values(1) - temperature value in K. (low range)
{*           Sensor_values(2) - temperature value in K. (high range)
{*           Sensor_values(3) - pressure value in PSIA.
{*           Sensor_values(4) - differential pressure value in mBar.
{*           Sensor_coeffs(1) - inner diameter of pipe in mm.
{*           Sensor_coeffs(2) - inner diameter of venturi throat in mm.
{*           Sensor_coeffs(3) - temperature breakpoint in K.
{*
{*   Implicit Inputs:
{*           convfact1 - conversion factor for PSIA to PASCAL.
{*           convfact2 - conversion factor for mBar to PASCAL.
{*           alpha_ss - thermal-expansion coefficient for SS.
{*
{*   Implicit Outputs:
{*
{*   Routine Status/Completion Codes:
{*
{*   Side Effects:
{*
{*   Notes:
{*           Reynold's number assumed to be initially 1.0E5.
{*           The massflow calculation is iterated until the
{*           reynold's number converges to within 10%.
{*
{**********}
function heflow_vent
             (var sensor_count: [readonly]integer;
              var sensor_values: [readonly]packed array
                              [$l1..$u1: integer] of real;
              var sensor_coeffs: [readonly]packed array
                              [$l2..$u2: integer] of real):
             real;

     label
             9999;                    { Error exit }

     var
             temp_high, temp_low: real;       { temperature values }
             temp_bkpt: real;                 { temperature breakpoint }
             temp,press,deltap: real;         { sensor values }
             tau: real;                       { ratio of p2 to p1 }
             idpipe, idthroat: real;          { sensor coefficients }
             dens: real;                      { density KG m**-3 }
             mflow: real;                     { mass flow KG/s }
             ReD: real;                       { Reynold's number }
             diffReD: real;                   { (ReD - newReD)/newReD }
             newReD: real;                    { new calculated value of ReD }
             eta: real;                       { Viscosity N s m**-2 }
             C: real;                         { Discharge coefficient }
             alpha: real;                     { Flow coefficient }
             expan: real;                     { Expansion factor }
             beta: real;                      { ratio of d to D }
             aread: real;                     { area of throat }
             m: real;                         { beta squared }
             cp, cv: real;                    { Cp and Cv }
             gamma: real;                     { Isentropic exponent }
             a: real;                         { constant in alpha }
             F: real;                         { Thermal-expansion factor }
```

```
begin   {function heflow_vent}

        { Initialize input parameters }

        temp_low := sensor_values[1];
        if temp_low < 2.Ø then
                temp_low := 2.Ø;

        temp_high := sensor_values[2];
        if temp_high < 2.Ø then
                temp_high := 2.Ø;

        press := sensor_values[3];
        if press <= press_min then
                begin
                heflow_vent := Ø.Ø;
                goto 9999;
                end;

        deltaP := sensor_values[4];
        if deltap <= Ø.Ø then
                begin
                heflow_vent := Ø.Ø;
                goto 9999;
                end;

        idpipe := sensor_coeffs[1];
        idthroat := sensor_coeffs[2];
        temp_bkpt := sensor_coeffs[3];

        { Conversions and factors }

        if temp_high <= temp_bkpt then
                temp := temp_low
        else
                temp := temp_high;

        beta := idthroat/idpipe;          { calc ratio of d to D }
        m := beta**2;                     { m = beta squared }
        aread := ((idthroat/1ØØØ.Ø)**2)*pi/4.Ø;
                                          { area of throat m**2 }
        deltap := convfact2*deltap;       { Convert mBar to Pascal }
        press := convfact1*press;         { Convert PSIA to Pascal }
        tau := (press-deltap)/press;      { ratio of p2 to p1 }
        dens := dfun (press, temp);       { Heprop density KG/M**3 }
        eta := visc (dens,temp);          { Heprop viscosity N s M**-2 }
        cp := csubp (temp,press);         { Calculate Cp }
        cv := csubv (temp,press);         { Calculate Cv }
        gamma := cp/cv;                   { calc isentropic exponent }
        ReD := 1.ØE5;                     { Start ReD = 1ØØØØØ }
        F := 1 + 2* alpha_ss*(temp - 293.15);
                                          { Thermal-expansion factor }
        { Check for errors }
        if (dens < Ø.Ø) or (eta < Ø.Ø) or (cp < Ø.Ø)
                or (cv < Ø.Ø) then
                begin
                heflow_vent := -9999.9;
                goto 9999;
                end;

        { Discharge coefficient for venturi ISO 5167-198Ø }
        C := Ø.995;                 { Assumes 1.ØE5 < ReD < 1.ØE6 }

        { Flow coefficient for venturi ISO 5167-198Ø }
        alpha := C * (1 - beta**4.Ø)**(-Ø.5);

        { Expansibility (expansion) factor ISA nozzles ISO 5167-198Ø }
        expan := ((gamma*tau**(2/gamma)/(gamma-1))*
                ((1-beta**4.Ø)/(1-(beta**4.Ø)*tau**(2/gamma)))*
                ((1-tau**((gamma-1)/gamma))/(1-tau)))**Ø.5;
```

```
            { Calculation of mass flow (Kg/s) }
            mflow := alpha*F*expan*aread*(2.Ø*dens*deltap)**Ø.5;

            { Calculate new value of Reynold's number }
            newReD := mflow*4/(pi * eta * (idpipe/1ØØØ.Ø));
            diffReD := (ReD-newReD)/newReD;

            heflow_vent := mflow * 1ØØØ.Ø;  { massflow in g/s }
9999:
     end;   {function heflow_vent}
```

```
{**********}
{*
{*      Function heatflow_orif: real;
{*
{*      Functional Description:
{*              This function calculates the heat flow between two locations
{*              in the LCTF helium system using the helium mass flow
{*              calculated from the heflow_orif function at one location
{*              and the temperature and pressure at both locations.
{*              The enthalpy is calculated at both locations and the
{*              difference in enthalpy is then used to calculate the
{*              heatflow in J/s (Watts) which is returned as the function
{*              value.
{*
{*      Formal Parameters:
{*              Sensor_count - integer number of sensor values used (7).
{*              Sensor_values(1) - low temperature (K) at location 1.
{*              Sensor_values(2) - high temperature (K) at location 1.
{*              Sensor_values(3) - pressure (PSIA) at location 1.
{*              Sensor_values(4) - low temperature (K) at location 2.
{*              Sensor_values(5) - high temperature (K) at location 2.
{*              Sensor_values(6) - pressure (PSIA) at location 2.
{*              Sensor_values(7) - differential pressure (mBar) at location 1.
{*              Sensor_coeffs(1) - inner diameter of pipe in mm.
{*              Sensor_coeffs(2) - inner diameter of orifice throat in mm.
{*              Sensor_coeffs(3) - temperature breakpoint (K).
{*
{*      Implicit Inputs:
{*              convfact1 - conversion factor for PSIA to PASCAL.
{*              convfact2 - conversion factor for mBar to PASCAL.
{*
{*      Implicit Outputs:
{*
{*      Routine Status/Completion Codes:
{*
{*      Side Effects:
{*
{*      Notes:
{*
{**********}
function heatflow_orif
                (var sensor_count: [readonly]integer;
                 var sensor_values: [readonly]packed array
                                [$l1..$u1: integer] of real;
                 var sensor_coeffs: [readonly]packed array
                                [$l2..$u2: integer] of real):
                real;

        label
                9999;                           { Error exit }

        var
                temp1_high,temp1_low,temp2_high,temp2_low,temp_bkpt: real;
                temp1, press1, temp2, press2, deltap: real;
                dens1, dens2, mflow: real;
                idpipe, idthroat: real;
                enthalpy1, enthalpy2: real;
                value: packed array[1..4] of real;
                coeff: packed array[1..3] of real;

        begin   {function heatflow_orif}
                { Initialize variables }

                temp1_low := sensor_values[1];
                temp1_high := sensor_values[2];
                press1 := sensor_values[3];
                temp2_low := sensor_values[4];
                temp2_high := sensor_values[5];
                press2 := sensor_values[6];
                deltaP := sensor_values[7];
                temp_bkpt := sensor_coeffs[3];

                { Determine which temperature to use in region 1 }
                if temp1_high <= temp_bkpt then
                        temp1 := temp1_low
```

```
            else
                    temp1 := temp1_high;

            { Determine which temperature to use in region 2 }
            if temp2_high <= temp_bkpt then
                    temp2 := temp2_low
            else
                    temp2 := temp2_high;

            { Check for possible bad data }
            if (deltaP < Ø.Ø) or (press1 < Ø.Ø) or (press2 < Ø.Ø ) or
               (temp1 < Ø.Ø) or (temp2 < Ø.Ø) then
                    begin
                    heatflow_orif := Ø.Ø;
                    goto 9999;
                    end;

            { Set up arrays for calling heflow routine }
            value[1] := temp1_low;
            value[2] := temp1_high;
            value[3] := press1;
            value[4] := deltaP;

            coeff[1] := sensor_coeffs[1];
            coeff[2] := sensor_coeffs[2];
            coeff[3] := sensor_coeffs[3];

            { Calculate helium massflow from orifice at position 1 }
            mflow := heflow_orif (4, value, coeff);
                                          { units of g/s }

            { Convert pressure units }
            press1 := convfact1*press1;      { pressure in Pascal }
            press2 := convfact1*press2;      { pressure in Pascal }

            { Calculate densities at position 1 and 2 }
            dens1 := dfun (press1,temp1);    { density from HEPROP }
            dens2 := dfun (press2,temp2);    { density from HEPROP }
                                          { units of KG/M**3 }

            { Calculate enthalpies at position 1 and 2 }
            enthalpy1 := hfun (dens1,temp1);{ enthalpy from HEPROP }
            enthalpy2 := hfun (dens2,temp2);{ enthalpy from HEPROP }
                                          { units of J/Kg }

            { Calculate heatflow from position 1 to 2 }
            heatflow_orif := mflow * (enthalpy2-enthalpy1)/1ØØØ.Ø;
                                          { units of J/s=Watts }
9999:
        end;    {function heatflow_orif}
```

ORNL/TM-9992
Dist. Category UC-20

INTERNAL DISTRIBUTION

1–5. L. R. Baylor
6. L. A. Berry
7. C. Bridgman
8. R. D. Burris
9. S. K. Combs
10. L. Dresner
11. B. C. Duggins
12. W. A. Fietz
13. W. M. Fletcher
14. R. D. Foskett
15. C. A. Foster
16. P. N. Haubenreich
17. P. H. Hight
18. T. Kato
19. M. S. Lubell
20. J. W. Lue
21. J. N. Luton
22. T. McManamy
23. C. S. Meadors
24. S. L. Milora
25. K. Okuno
26. T. L. Ryan
27. S. W. Schwenterley
28. S. S. Shen
29. J. Sheffield
30. W. D. Shipley
31. R. E. Stamps
32. A. Ulbricht
33. F. Wuechner
34. R. B. Wysor
35. J. Zichy
36–37. Laboratory Records Department
38. Laboratory Records, ORNL-RC
39. Document Reference Section
40. Central Research Library
41. Fusion Energy Division Library
42. Fusion Energy Division Publications Office
43. ORNL Patent Office

EXTERNAL DISTRIBUTION

44. Office of the Assistant Manager for Energy Research and Development, U.S. Department of Energy, Oak Ridge Operations, Box E, Oak Ridge, TN 37831
45. V. D. Arp, National Bureau of Standards, Boulder, CO 80302
46. M. P. G. Avanzini, Nucleare Italiana Reattori Azanzati, C.P. 1166, 16100 Genova, Italy
47. D. S. Beard, Office of Fusion Energy, Department of Energy, Washington, DC 20545
48. G. Bogner, Forschungslaboratorien, Aktiengesellschaft, Postfach 325, D-8520 Erlanger 2, Federal Republic of Germany
49. J. D. Callen, Department of Nuclear Engineering, University of Wisconsin, Madison, WI 53706
50. A. Clark, National Bureau of Standards, Boulder, CO 80302
51. J. F. Clarke, Associate Director for Fusion Energy, Office of Energy Research, ER-50 Germantown, U.S. Department of Energy, Washington, DC 20545
52. D. L. Coffey, American Magnetics, Inc., P.O. Box R, Oak Ridge, TN 37830
53. E. W. Collings, Battelle Memorial Institute, 505 King Avenue, Columbus, OH 43201
54. R. W. Conn, Department of Chemical, Nuclear, and Thermal Engineering, University of California, Los Angeles, CA 90024
55. S. O. Dean, Director, Fusion Energy Development, Science Applications International Corporation, 2 Professional Drive, Suite 249, Gaithersburg, MD 20879
56. H. Desportes, STIPE, CEN/Saclay, B.P. 2, F91190, Gif-sur-Yvette, France

57. G. W. Donaldson, School of Electrical Engineering, University of New South Wales, P.O. Box 1, Kensington, N.S.W. 2033, Australia
58. R. W. Fast, Manager, Experimental Facilities, Fermi National Accelerator Laboratory, P.O. Box 500, Batavia, IL 60510
59. F. Fickett, National Bureau of Standards, Boulder, CO 80302
60. J. File, Princeton Plasma Physics Laboratory, P.O. Box 451, Princeton, NJ 08540
61. H. K. Forsen, Bechtel Group, Inc., Research Engineering, P.O. Box 3965, San Francisco, CA 94105
62. Y. Furuto, Chief, Superconducting Group, Central Research Laboratory, Furukawa Electric Co., Ltd., 9-15, 2-Chome, Futuba, Shinagawa, Tokyo 141, Japan
63. W. F. Gauster, c/o H. Kirchmayr, Director, Institut für Experimentalphysik der Technischen Hochschule in Wien, Karlsplatz 13, A-1040 Vienna, Austria
64. J. R. Gilleland, GA Technologies, Inc., Fusion and Advanced Technology, P.O. Box 81608, San Diego, CA 92138
65. R. W. Gould, Department of Applied Physics, California Institute of Technology, Pasadena, CA 91125
66. E. Gregory, Airco Syperconductors, 600 Milik St., Carteret, NJ 07008
67. R. A. Gross, Plasma Research Laboratory, Columbia University, New York, NY 10027
68. D. S. Hackley, General Dynamics–Convair Division, P.O. Box 80847, San Diego, CA 92138
69. R. Hancox, UKAEA, Culham Laboratory, Abingdon, Oxon OX14 3DB, United Kingdom
70. W. Heinz, Institut für Experimental Kernphysik, Kernforschurgezentrum Postfach 3640, D-7500 Karlsruhe 1, Federal Republic of Germany
71. C. D. Henning, Lawrence Livermore National Laboratory, P.O. Box 808, Livermore, CA 04550
72. R. L. Hirsch, Deputy Manager, Science and Technology Division, Exxon Corporation, 1251 Avenue of the Americas, New York, NY 10020
73. M. O. Hoenig, Francis Bitter National Magnet Laboratory, 170 Albany Street, Cambridge, MA 02139
74. R. Huse, Manager, Research and Development Department, PSE&G Research Corporation, 80 Park Place, Newark, NJ 07101
75. M. Iwamoto, Central Research Laboratory, Mitsubishi Electric Corporation, 80 Nakano, Minamishimizu, Amagasaki, Hyogo 660, Japan
76. C. K. Jones, Cryogenic Research Laboratory, Research and Development Center, Westinghouse Electric Corporation, Pittsburgh, PA 15235
77. A. Knobloch, Max-Planck-Institut für Plasmaphysik, Abteilung Technik, D-8046 Garching, Federal Republic of Germany
78. P. Komarek, Institut für Experimental Kernphysik, Kernforschurgezentrum Karlsruhe Postfach 3640, D-7500 Karlsruhe 1, Federal Republic of Germany
79. K. Koyama, Electrotechnical Laboratory, 5-4-1 Mukodai-cho, Tanashi-City, Tokyo, Japan
80. G. L. Kulcinski, Nuclear Engineering Department, 1500 Johnson Drive, University of Wisconsin, Madison, WI 53706
81. K. Kuroda, Hitachi, Ltd., Central Research Laboratory, 1-280, Higa Shiko Igakubo, Kokubumji, Tokyo 185, Japan
82. J. C. Lottin, CEN/Saclay, Department du Synchrotron Saturne, B.P. 2, 91190 Gif-sur-Yvette, France
83. F. Moon, Department of Theoretical and Applied Mechanics, Cornell University, Ithaca, NY 14850
84. T. Ogasawara, Department of Physics, College of Science and Engineering, Nihon University, Kanda-Surugadai, Chiyoda-ku, Tokyo, Japan

85. H. Ogiwara, Toshiba Research and Development Center, 1 Komukai Tsohibacho, Saiwai-ku, Kawasaki, Kanagawa 210, Japan
86. F. Prevot, CEN/CADARAHE, Department de Recherches sur la Fusion Controllee, 13108 Saint-Paul-Lez-Durance, Cedex, France
87. L. K. Price, Energy Programs and Support Division, Department of Energy, Oak Ridge Operations, P.O. Box E, Oak Ridge, TN 37831
88. M. Roberts, International Programs, Office of Fusion Energy, Office of Energy Research, ER-52 Germantown, U.S. Department of Energy, Washington, DC 20545
89. D. J. Rose, Department of Nuclear Engineering, Massachusetts Institute of Technology, Cambridge, MA 02139
90. G. Sacerdoti, Laboratorio Nazionali, Casella Postale 70, 00044 Frascari (Roma), Italy
91. S. St. Lorant, Stanford Linear Accelerator Center, Stanford University, Palo Alto, CA 94304
92. Y. Sawada, Advanced Engineering Group, Heavy Apparatus Engineering Laboratory, Tokyo Shibaura Electric Company, Ltd., 4-2-Chome, Suehiro-cho, Tsurumi-ku, Yokohama, Japan
93. K. Schmitter, Max-Planck-Institut für Plasmaphsik, D-8046 Garching, Federal Republic of Germany
94. J. Schultz, Plasma Fusion Center, 167 Albany Street, Cambridge, MA 02139
95. S. Shimamoto, Japan Atomic Energy Research Institute, Tokai Research Establishment, Tokai, Ibaraki, Japan
96. M. Spadoni, Laboratorio Nazionali, Casella Postale 70, Frascati (Roma), Italy
97. W. M. Stacey, School of Nuclear Engineering, Georgia Institute of Technology, Atlanta, GA 30332
98. D. Steiner, Rensselaer Polytechnic Institute, Nuclear Engineering Department, NES Building, Tibbets Avenue, Troy, NY 12181
99. B. P. Strauss, Magnetic Corporation of America, 179 Bear Hill Road, Waltham, MA 02154
100. K. Tachikawa, Electric Materials Laboratory, National Research Institute for Metals, 3-12, 2-Chome, Nakameguro, Meguru-ku, Tokyo, Japan
101. D. T. Uchida, Nuclear Engineering Department, University of Tokyo, Tokyo, Japan
102. S. Vécsey, Swiss Institute for Nuclear Research, CH-5234 Villigen, Switzerland
103. C. Walters, Technology Division, Bldg. R25, Rutherford and Appleton Laboratories, Chilton, Didcot, Oxon OX 11 OQX, United Kingdom
104. M. Wilson, Rutherford and Appleton Laboratories, Chilton, Didcot, Oxon OX11 OQX, United Kingdom
105. S. L. Wipf, Q-26, Los Alamos National Laboratory, P.O. Box 1663, Los Alamos, NM 87545
106. H. H. Woodson, Department of Electrical Engineering, University of Texas, Austin, TX 78712
107. M. Yamamoto, Toshiba, Tsurumi Works, 4-2-Chome Suehiro-cho, Tsurumi-ku, Yokohama 230, Japan
108. K. Yasukochi, Department of Physics, College of Science and Engineering, Nihon University, Kanda-Surugadai, Chiyoda-ku, Tokyo, Japan
109. R. Varma, Physical Research Laboratory, Navrangpura, Ahmedabad 380009, India
110. Bibliothek, Max-Planck Institut für Plasmaphysik, D-8046 Garching, Federal Republic of Germany
111. Bibliothek, Institut für Plasmaphysik, KFA, Postfach 1913, D-5170 Jülich, Federal Republic of Germany
112. Bibliotheque, Centre de Recherches en Physique des Plasmas, 21 Avenue des Bains, 1007 Lausanne, Switzerland

113. Documentation S.I.G.N., Departement de la Physique du Plasma et de la Fusion Controlee, Centre d'Etudes Nucleaires, B.P. No. 85, Centre du Tri, 38041 Cedex, Grenoble, France
114. Library, Culham Laboratory, UKAEA, Abingdon, Oxfordshire, OX14 3DB, England
115. Library, FOM Institut voor Plasma-Fysica, Rijnhuizen, Jutphaas, The Netherlands
116. Library, Institute of Plasma Physics, Nagoya University, Nagoya 64, Japan
117. Library, International Centre for Theoretical Physics, Trieste, Italy
118. Library, Laboratorio Gas Ionizzati, Frascati, Italy
119. Library, Plasma Physics Laboratory, Kyoto University, Gokasho Uji, Kyoto, Japan
120. Plasma Research Laboratory, Australian National University, P.O. Box 4, Canberra, A.C.T. 2000, Australia
121. Thermonuclear Library, Japan Atomic Energy Research Institute, Tokai, Naka, Ibaraki, Japan

122–230. Given distribution as shown in TIC-4500 Magnetic Fusion Energy (Category Distribution UC-20)